Relation Between Storm Characteristics and Extreme Precipitation Statistics Over CONUS

Diogo Araujo[a], Francesco Marra[b,c], Haider Ali[d], Hayley J. Fowler[d,e], Efthymios I. Nikolopoulos[a*]

[a]*Department of Civil and Environmental Engineering, Rutgers University, Piscataway, NJ, USA*

[b]*Department of Geosciences, University of Padova, Italy*

[c]*Institute of Atmospheric Sciences and Climate, National Research Council (CNR-ISAC), Bologna, Italy*

[d]*School of Engineering, Newcastle University, UK*

[e]*Tyndall Centre for Climate Change Research, Newcastle University, UK*

[*]Corresponding author: Efthymios I. Nikolopoulos
(efthymios.nikolopoulos@rutgers.edu)

Abstract

In this paper we use a statistical framework to analyze the relation between storm properties and the statistics of extreme precipitation. We identify storm events using a 24-hour dry hiatus separation. We investigate the statistics of the hourly maximum intensity for the heaviest storm events at durations of 1 and 24 h. A two-parameter Weibull distribution is used to represent precipitation frequencies at several stations from a quality-controlled hourly precipitation dataset over the contiguous United States, encompassing seven climate zones. The Spearman correlation between the distribution parameters and a selection of storm properties (duration, intensity, decorrelation time, convective-like ratio) and station properties (elevation and latitude) is used to measure the relation of these properties with the statistics of extreme precipitation. Our results indicate that observed annual maximum hourly precipitation over the entire study area are likely samples from the used distribution, implying that a two-parameter Weibull distribution is suitable for modeling hourly and 24-hour precipitation extremes over the contiguous United States. The spatial variability of shape parameters obtained for hourly events showed lighter tails in the west coast when compared to the rest of CONUS, while the central-north displays heavier tails. We identify statistically significant links (at the 95% confidence level) between storm characteristics connected with the underlying processes (e.g., typical storm duration, typical temporal autocorrelation, proportion of convective-like storms) and the parameters of the distribution. Notably, characteristics typical of convective precipitation, e.g., sharp decorrelation time and high hourly intensity, tend to be related to distributions with heavier tails. These results provide a first step towards linking the characteristics of storms with the local statistics of extremes.

Keywords: precipitation extremes, frequency analysis, storm characteristics.

1. Introduction

Quantifying and characterizing hydrometeorological extremes is of foremost importance when dealing with hydrological hazards and climate change adaptation strategies. According to National Oceanic and Atmospheric Administration (NOAA) (2022), the United States suffered $2,278.2 billion dollars in losses due to natural disasters from 1980 to July 2022. Tropical cyclones ($1,194.4 billion, 52.4%), severe storms ($365.3 billion, 16%), and droughts ($300.1 billion, 13.2%) represent the three extreme weather categories producing higher costs. NOAA (2022) also indicates an increase in the number of billion-dollar events per year, from 3.1 in 1980-1989, to 17.8 in the last 5 years (2017-2021). Aside from financial impacts, these natural disasters have caused 15,355 deaths since 1980. Several studies based on future projections from Global Circulation Models (GCMs) indicate that the number of extreme precipitation events in the United States is projected to increase towards the end of the 21st century (Cooley & Chang, 2020; Lopez-Cantu et al., 2020; Prein et al., 2016; Zhu Jianting, 2013).

Hydro-meteorological extremes are usually assessed by the frequency analysis of precipitation data. The frequency of exceedance of very large precipitation amounts is commonly modeled using probability distributions fitted to precipitation extremes from gauges, satellites or atmospheric models (Hu et al., 2020). This procedure allows for the extrapolation of very rare events that are potentially not represented in the observations. A common basis for this approach is extreme value theory, which relies on two main assumptions: the events are independent and identically distributed; and the extremes are intended as maxima of asymptotically large blocks(practically, the number of events in each year is large enough to be assumed infinite, $n \rightarrow \infty$). Alternatively, Poisson exceedances of an asymptotically high threshold can be examined (Fisher & Tippett, 1928; Gnedenko, 1943). This asymptotic assumption constitutes an important theoretical hindrance to establishing relations linking the physical processes bringing precipitation to a given region (i.e., the finite number of storms with given characteristics that hit the area) and the emerging statistics of extremes. Other approaches can be used, such as the identification and use of the best fitting among various probability distribution families. While these probability distributions are not based on asymptotic theory, they are characterized by the same drawbacks that we detail below.

The small data samples constituted by the observed/modeled extremes result in large uncertainties on the estimated probability distributions (Katz et al., 2002; Serinaldi & Kilsby, 2014). These uncertainties have motivated the development of new approaches. This new concept assumes that extremes are samples from the so-called ordinary events, which are all the independent realizations of the stochastic process of interest (Marani & Ignaccolo, 2015; Marra et al., 2018; Schellander et al., 2019; Zorzetto et al., 2016). Naturally, these approaches explicitly separate the number of occurrences of storms from their magnitude distribution, e.g., see (Marra et al., 2020a) and thus implicitly include a direct relation between the underlying physics (the storms) and the emerging statistics.

Frequency analysis using asymptotic and non-asymptotic frameworks has been extensively applied in the literature to quantify changes to the quantiles of extreme events, either by comparing present and future time-slices, or by examining continuous changes or trends in space or time (Huang et al., 2022; Kunkel et al., 2020; Li et al., 2022;Marra et al., 2020b; Martinez-Villalobos & Neelin, 2018; Miniussi & Marani, 2020; Prein et al., 2016; Vidrio-Sahagún et al., 2023; Zhu Jianting, 2013). Another approach examines the causative relations between predictor variables (proxies) and the process of interest. These analyses are usually focused on describing the mechanism behind each process, in contrast to the frequency analysis developed by the probabilistic framework. For example, studies have analyzed the influence of latitude and elevation on the statistics of precipitation extremes (Amponsah et al., 2022; Papalexiou et al., 2018), as well as the influence of precipitable water (Kim et al., 2022), temperature (Barbero et al., 2018; Zhu et al., 2022) and orography (Formetta et al., 2022; Marra et al., 2021).

Approaches similar to the causative relation analysis can also be used to identify and quantify ongoing and future changes in extremes based on changes to the causative processes and in their properties (Dallan et al., 2022; Marra et al., 2021; Marra et al., 2019; Vidrio-Sahagún & He, 2022). As this is based on physical understanding rather than mere statistical extrapolation, these approaches may enable a more robust prediction of future extremes. Analyses performed so far, however, have considered only a small number of factors (e.g., latitude, elevation, or temperature) and have not enabled the identification of a direct link between storm properties (such as hourly intensity, decorrelation time and duration) and statistics of extremes. To the best of our knowledge, a robust assessment of the relation between typical storm properties and a statistical description of precipitation extremes is still missing in the current literature. However, using the statistics of ordinary events based on storm objects allows us to do such analysis, identifying important proxies that could influence the behavior of precipitation extremes. These proxies provide insights on the formation processes behind extreme precipitation and, in addition to improving the overall understanding of tail behavior over CONUS, can enhance modeling exercises.

This study investigates the relation between several storm and geographic characteristics (duration, maximum intensity, mean intensity, decorrelation time, elevation, latitude, and fraction of convective events) and the statistics of hourly and daily extreme precipitation. Our specific goals were to: (i) validate the applicability of the Weibull distribution for modeling precipitation extremes over CONUS, (ii) analyze the spatial patterns of the distribution parameters over different climatic zones, and (iii) investigate the possible relations between different storm characteristics and the distribution parameters (i.e., statistics of extremes).

2. Data and Study Area

2.1. Characteristics of the region

The study area consists of the contiguous United States (CONUS) (Figure 1). The region covers an extensive territory constrained between latitudes 25-50ºN, and longitudes 60-130ºW. The precipitation distribution drastically varies across CONUS. The states along the eastern coast and Gulf are influenced by tropical cyclones in late summer and early fall (Knight & Davis, 2007). The western coast is dominated by Pacific storms during the winter season (Moore et al., 2021). Precipitation events in southern areas and over the Great Plains are influenced by the North American monsoon during summer (Higgins et al., 1997). El Niño and La Niña also have a significant influence on rainfall patterns over CONUS, especially over the West, Midwest and Southeast (Gershunov, 1998).

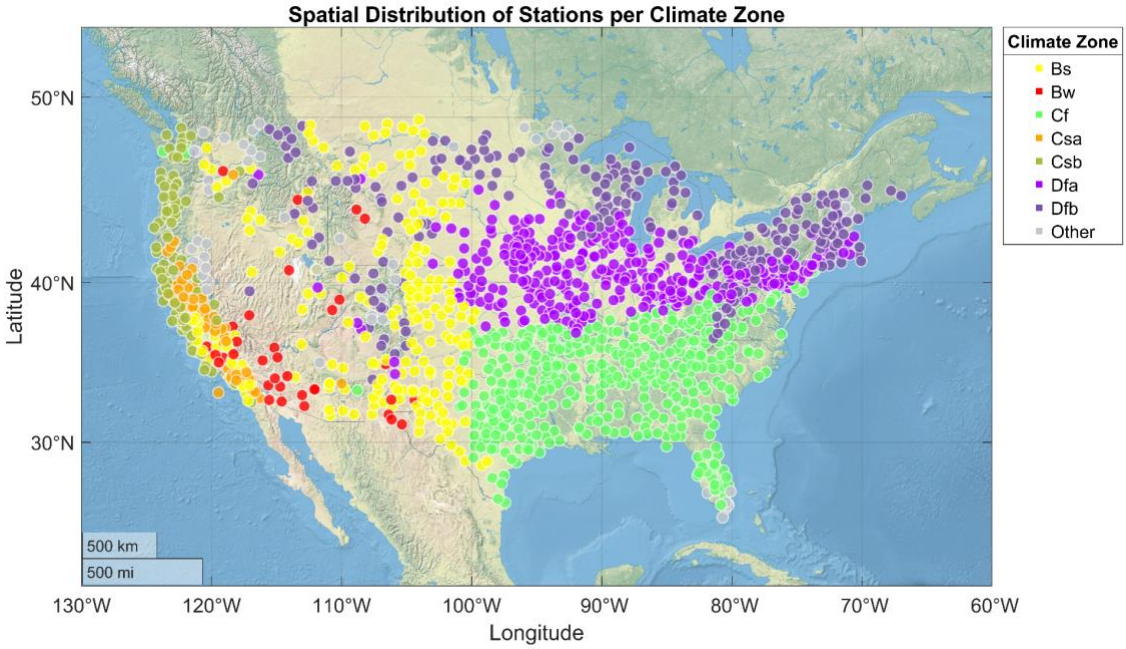

Figure 1 - Spatial distribution of stations per climate zone according to the Köppen-Geiger classification (Peel et al., 2007)

Table 1 - Climate Zones over CONUS modified from (Peel et al., 2007).

Climate Zone	Description	Location
BS	Arid Steppe climate	Covers most of the Great Plains, east of the Rocky Mountains
BW	Arid Desert climate	Covers areas the Death Valley National Park and some locations around the Rocky Mountains
Cf	Temperate climate without dry season	Encompasses the southeastern areas of CONUS

Csa	Temperate climate with dry and hot summer	Located on the entire coast of California
Csb	Temperate climate with dry and warm summer	Located on the south portion of the California coast
Dfa	Cold climate without dry season and hot summer	Located east of the Great Plains around 40ºN latitudes
Dfb	Cold climate without dry season and warm summer	Includes the areas of New England, parts of the Rocky and Appalachian Mountains

The statistics of extreme precipitation emerge from the interaction of different weather systems with local features and terrain conditions (Marra et al., 2021; Mazzoglio et al., 2022; Papalexiou et al., 2018). To better understand the relations between storm properties and emerging extremes in an area as vast as the CONUS, it is thus useful to separately examine regions with different climatology. According to the updated Koppen-Geiger maps (Peel et al., 2007), more than 20 different climate zones are found within CONUS. In this study, the climate zones were grouped into seven main categories (Table 1) based on the availability of sufficient gauge stations (with at least 30 stations in each zone). The climate zones with less than 30 stations were clustered in a category named "Other".

2.2. Data and quality control

We used hourly precipitation from the Global Sub-Daily Rainfall (GSDR) observational dataset (Lewis et al., 2019). The GSDR dataset is the result of an effort from the European Research Council-funded INTENSE project ('INTElligent use of climate models for adaptatioN to non-Stationary hydrological Extremes') (Blenkinsop et al., 2018) in collecting sub-daily rainfall observations around the world. The complete global dataset consists of 24,394 gauge stations with hourly precipitation data of varying resolution (e.g., 2.5 mm, 0.25 mm), record length (spanning from <1 to 104 years), spatial coverage, completeness and quality (Lewis et al., 2021). In this study, we used a version of the GSDR dataset that was corrected to solve for quality issues, such as equipment malfunctions and recording errors (Ali et al., 2021, 2022; Lewis et al., 2021). The correction algorithm, named GSDR-QC, is based on a routine with 25 quality checks that is used to remove errors in data, being adaptable to incorporate regional information.

Additional constraints and quality control criteria were used to screen the stations in this study: (i) only stations within CONUS boundaries were considered, i.e., within latitudes 25-50ºN, and longitudes 60-130ºW; (ii) years in which data is stored with 2.5 mm measurement resolution were discarded; (iii) years with more than 10% missing data were discarded; (iv) stations with less than 20 years of record were removed from the analysis; (v) stations in which the hypothesis test for Weibull tail (Section 3.2) was rejected (57 stations) were removed. It is

important to note that this represents a very small rejection rate (~3.6%), which is fully explained by type I errors (see Marra et al., 2022 and Marra et al., 2023). After these additional criteria had been applied, 1,530 stations were used in the study. They are divided among the climate types: BS (217), BW (35), Cf (439), Csa (71), Csb (73), Dfa (357), Dfb (254) and Others (84). Their spatial distribution can be seen in Figure 1.

3. Methods

Statistics of heavy precipitation were described using a two-parameter Weibull distribution (stretched exponential). The concept of 'ordinary events', described as all independent realizations of the process of interest (Marra et al., 2020b) was used to perform the parameter estimation and representation of such process. This definition, along with the left-censoring described in section 3.2., helped to identify those events associated with precipitation extremes, from which the characteristics used in this study were derived.

3.1. Statistical framework

Following the unified approach proposed in Marra et al. (2020), we based the identification of ordinary events on the concept of storms, which are defined as wet time-intervals separated by dry hiatuses of at least 24h length. In that sense, precipitation amounts separated by less than 24h are considered in the same storm event even if they are discontinuous. After identifying the storms, ordinary events are defined as the hourly maximum intensities within each storm using two time windows, 1h and 24h. This definition allows for the direct comparison of storm properties and model parameters across different storm durations, because the number of ordinary events is equal to the number of storms and is thus the same for all durations. This provides a direct correspondence between meteorological objects (the storms, and therefore their properties) and the emerging statistical parameters (Marra et al., 2020b). In the context of extreme daily precipitation, these independent ordinary events were often defined as precipitation amounts on wet days, and modeled with a stretched exponential (two-parameter Weibull) distribution (Marani & Ignaccolo, 2015; Miniussi et al., 2020; Zorzetto et al., 2016). Recent studies based on theoretical formulations and gauge observations, however, indicate that only the upper tail of the ordinary events distribution is accurately modeled by the stretched exponential distribution (Amponsah et al., 2022; Marani & Ignaccolo, 2015; Marra et al., 2023, 2020b, 2018, 2019; Miniussi & Marra, 2021; Miniussi et al., 2020; Vidrio-Sahagún & He, 2022; Zorzetto et al., 2016). This portion of ordinary events, that we term here "tail", can be identified using a left-censoring threshold (See section 3.2). An optimal choice of such threshold assures the best representation of the tail statistics (Marra et al., 2023). The tail defined by this optimal left-censoring threshold can incorporate large portions of the timeseries, e.g., above 60^{th} percentile. Its definition implies that the annual maxima (i.e., the traditional quantity used to define extremes) are sampled from this distribution. Figure S6 in the supplementary information illustrates the left-censoring and fitting process.

Following previous applications (Marani & Ignaccolo, 2015; Marra et al., 2018), the tail of the ordinary events distribution is modeled using a Weibull distribution, which can be described by its cumulative distribution function below:

$$F(x;\lambda,\kappa) = 1 - e^{-(\frac{x}{\lambda})^{\kappa}} \quad \text{(eq. 1)}$$

The coefficients λ and $\kappa \in]0,\infty[$ are the scale and shape parameters, respectively. The scale parameter is a parameter such that $F(x;\lambda) = F(x/\lambda;1)$, while the shape parameter determines the skewness of the distribution, providing a direct interpretation of the tail heaviness and consequently important information on the extremes, i.e., larger shape parameters indicate lighter tails and vice-versa.

3.2. Identification of the optimal left-censoring thresholds

In order to represent the tail of the distribution, ordinary events need to be left-censored. The optimal value of the left-censoring threshold depends on climate and can thus vary from case to case. Therefore, we performed a separate sensitivity analysis for the two time windows (1 and 24h) on all stations to identify its value. This analysis follows the Monte Carlo-based hypothesis test procedure proposed in Marra et al. (2020b) and described in detail in Amponsah et al. (2022), Marra et al. (2020b, 2022). Codes for this test are available in Marra (2022): (1) a left-censoring threshold is assumed to identify the distribution tail, e.g. the 80th percentile of the ordinary events; (2) the parameters of the Weibull distribution describing this tail are estimated by censoring (i) all the ordinary events below threshold and (ii) all the observed annual maxima (censoring means that we do not use the quantitative values for estimation but we retain the weight in probability, i.e., any j-th quantile will retain the same value after the censoring) and using a least-square regression in Weibull-transformed coordinates (e.g. see Marani & Ignaccolo, 2015); (3) 1000 stochastic samples are drawn from the estimated distribution; (4) the observed annual maxima are compared to the samples to check whether they are likely samples from the tested distribution. Full details about this test are reported in Marra et al. (2023). By definition, the optimal left-censoring thresholds are those thresholds above which the test never rejects the Weibull tails; consequently, there is no sensitivity of the estimated parameters to small variations of their value. Since the outcome of the test depends on the sampled annual maxima of each case, it is subject to some level of stochasticity. The thresholds, however, are a climatic property; therefore, we selected the optimal left-censoring threshold for each station as the median of the threshold values of stations within a 200 km radius.

3.3. Definition of storm characteristics

The top ten percent (the values exceeding the 90th percentile) of the storms associated with extreme events in all stations were identified for both time windows, 1h and 24h, i.e., two different sets of storms were obtained based on the 1- and 24-h maximum intensities. This common value was adopted to ensure consistency. From them, we derived the following climatic and geographic variables: (1) Duration of the storm event; (2) Maximum Intensity of the storm event; (3) Mean Intensity of the storm event; (4) Decorrelation time; (5) Gauge Station Elevation; (6) Gauge Station Latitude and (7) Ratio of convective-like storms. Each station has a single value for elevation, latitude and ratio of convective storms; conversely, to represent duration, maximum and mean intensities, and decorrelation time at the station level,

198 we used their mean values across the storms. The influence of the climatic variables on the tail
199 parameters were measured by the Spearman's correlation coefficient. A separate evaluation
200 was performed considering the climate zones independently. The characteristics of typical
201 storms used in this study are defined in Table 2.

202 Table 2 - Definition of storm characteristics

No.	Characteristic	Definition
1	Duration	Difference in time between the end and start of the storm, measured in hours
2	Maximum Intensity	Hourly Maximum rainfall intensity extracted from each storm, measured in millimeters per hour.
3	Mean Intensity	Average of rainfall intensities within each storm, measured in millimeters per hour.
4	Decorrelation Time	Time lag (in hours) at which the autocorrelation of hourly precipitation time series becomes smaller than e-1 (0.368).
5	Gauge elevation	Elevation of the gauge station relative to sea level, measured in meters.
6	Ratio of Convective-like Storms	Number of storms classified as convective (Section 3.4) divided by the total number of storms

203

204 ***3.4. Identification of convective-like storms***

205 We classified the storms based on proxies of the dominant physical process during their peak
206 hourly intensity. The systematic separation of convective and stratiform precipitation
207 components is still an open research question (Ghada et al., 2022; Sui et al., 2007; Thurai et
208 al., 2021; Treppiedi et al., 2022; Wang et al., 2021). Following previous studies (Dallan et al.,
209 2022), here we used a simplified approach based on macroscopic characteristics typical of
210 convective precipitation, which are the sharp temporal variability and the high intensity of the
211 emerging precipitation. We classify as 'convective-like' all storms with temporal decorrelation
212 time shorter or equal to 3 hours and maximum hourly intensity greater or equal to 3 mm/h
213 (Figure S5). It is worth noting that with respect to Dallan et al. (2022), for which sub-hourly
214 data was available, here we only have hourly time series. The temporal autocorrelation is thus
215 more difficult to evaluate, as the temporal scales of convection are typically around or even
216 below 1 hour. This implies that a proper optimization of these values is not feasible with the
217 dataset at hand. The values of 3 hour for decorrelation time and 3 mm/h for maximum hourly

intensity were thus chosen based on visual inspection. However, it is important to note that these values are well within the range indicated by other authors (Treppiedi et al., 2022).

Convective-like storms are expected to have their peak intensities dominated by convective processes. The remaining storms are classified as 'other' and are expected to have their peak intensities associated with different types of processes. Although this classification is somewhat crude, it is deemed sufficient here as we aim to evaluate the qualitative impact that the proportion of convective-like storms may have on the parameters of the emerging distributions, and we do so by using Spearman (rank) correlations.

4. Results and Discussion

4.1. Evaluation of statistical framework

The sensitivity test results indicate a good performance of the Weibull distribution in representing the tail statistics and annual maxima. Figure 3 reports the optimal left-censoring thresholds needed to identify the Weibull portion of the ordinary events distribution. We can see significant variability across CONUS, with thresholds ranging from near 0 (light blue dots on Figure 3), i.e., the entire ordinary events distribution is well approximated by a stretched exponential from which annual maxima are sampled, to the 90th percentile (red dots on Figure 3). Higher thresholds are needed for the 1-hour time window in the northeastern and western portions of CONUS, covering parts of Maine, New York, parts of the Appalachian and Rocky Mountains. The higher left-censoring threshold in areas with high elevation for short durations suggests an influence of orography. The area covered by the Great Plains presents middle range values, from the 20th to 70th percentile. The 24-hour time window (bottom panel of Figure 3) presents more stations associated with smaller thresholds (< 10th percentile), especially in the central portions of CONUS and the southern coast of California. Given the sensitivity and specificity of the test against alternative tail models, such as power-type tails and Generalized Pareto tails shown by Marra et al. (2023), the results in Figure 3 support the use of a stretched-exponential tail model also for hourly precipitation.

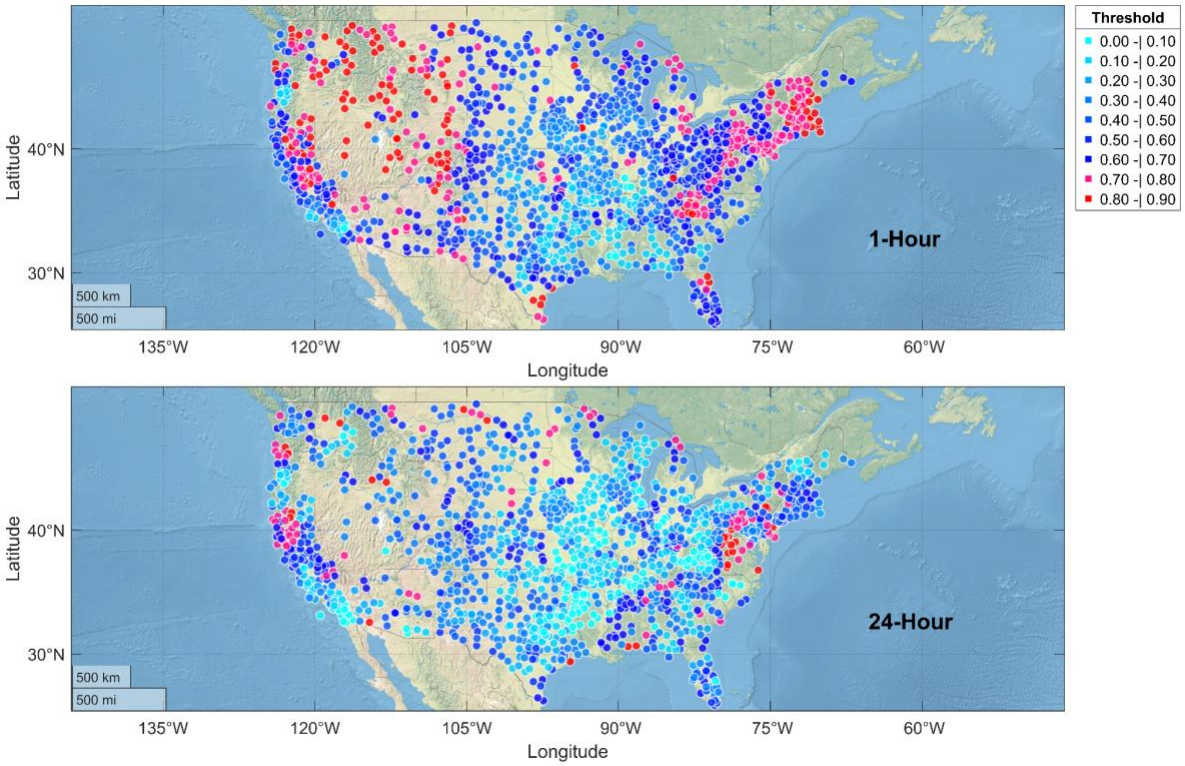

Figure 3 - Left-Censoring Threshold for tail definition of extremes at 1 and 24-hour time-windows. The optimal value corresponds to the threshold used to define the tail of the distribution, i.e., an optimal value of 0.90 indicates that values above the 90th percentile are considered to be in the tail. Lighter blue colors indicate smaller thresholds, darker blue indicate middle-range values and red colors represent higher values. The upper panel refers to values of 1-hour time window ordinary events, while the bottom panel displays results for 24-hour events.

A detailed investigation of the optimal left-censoring thresholds per climate zone is displayed in Figure 4. We can observe that for all climate zones the optimal values are consistently smaller for the longer duration against the shorter. The 1-hour median optimal value ranges from the 45th to 70th percentile, while the 24-hour ranges from the 30th to 50th for the seven climate zones considered. The climate zones BW and Dfb present higher threshold values for the 1-hour time window, which are significantly reduced for the 24-hour duration. These higher optimal values mean that a smaller portion of the ordinary events is included in the tail. The temperate climate zone (Cf) presents the smallest left-censoring values for 24-h and the second smallest for the 1-hour. This region is characterized by no dry season, i.e., it has a significant number of extreme events year-round, with a consequent larger proportion of the ordinary events belonging to the tail.

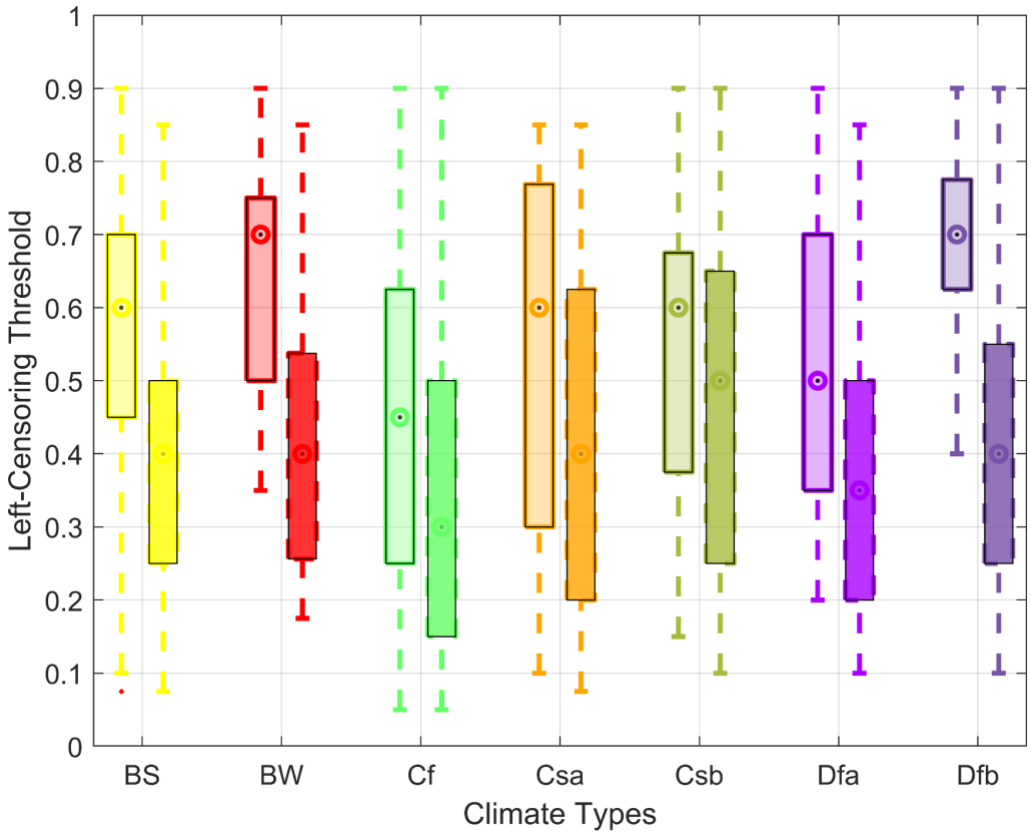

Figure 4 - Left-Censoring Threshold for tail definition of extremes for the different climate zones of CONUS. Light colors indicate values for 1-hour, while darker colors indicate 24-hour time window. The climate types are: BS (yellow) - Arid Steppe climate; BW (red) - Arid Desert climate; Cf (green) - Temperate climate without dry season; Csa (orange) - Temperate climate with dry and hot summer; Csb (dark green) - Temperate climate with dry and warm summer; Dfa (light purple) - Cold climate without dry season and hot summer; Dfb (dark purple) - Cold climate without dry season and warm summer.

The mean annual number of ordinary events (N) provides an insight into the occurrences of events across CONUS, as presented in Figure 5. The southwest and a significant part of the Great Plains have the smallest values of N, ranging from near 0 to 45 independent events/year. This result is consistent with the precipitation patterns in these regions, which are characterized by desert and an arid climate. In contrast, the northeast has the highest values in the study domain (60-90 events/year). The southeast and northwest regions have a similar mean annual number of events, ranging from 45 to 75 events/year. In general, values of N followed the expected patterns based on the rainfall climatology of CONUS.

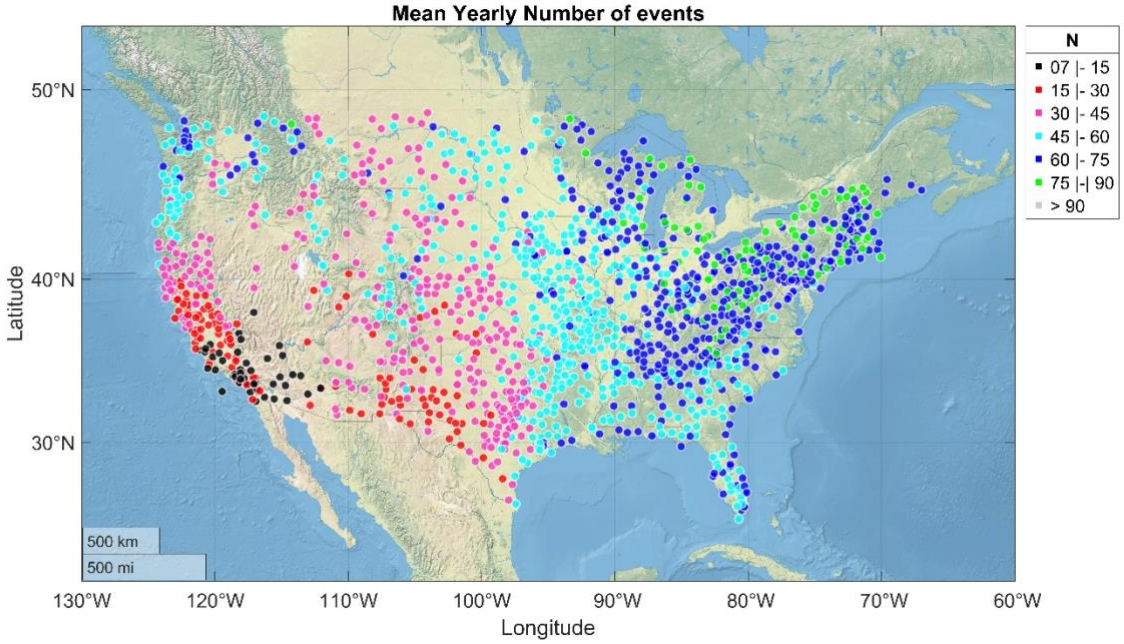

Figure 5 - Mean annual number of ordinary events (N) over CONUS.

4.2. Parameters of the Weibull distribution describing the tails

The definition of the tails, based on the left-censoring thresholds discussed above, allows us to describe the extremes using a two parameter Weibull distribution. The analysis of the two parameters (scale and shape) across regions allows important insights into the characteristics of extreme precipitation. The shape parameter in particular controls the skewness of the distribution, providing information about the tail heaviness, which represents the rate at which the occurrence probability decreases at increasing intensities. In the formulation in eq. (1), smaller values of the shape parameter indicate heavier tails.

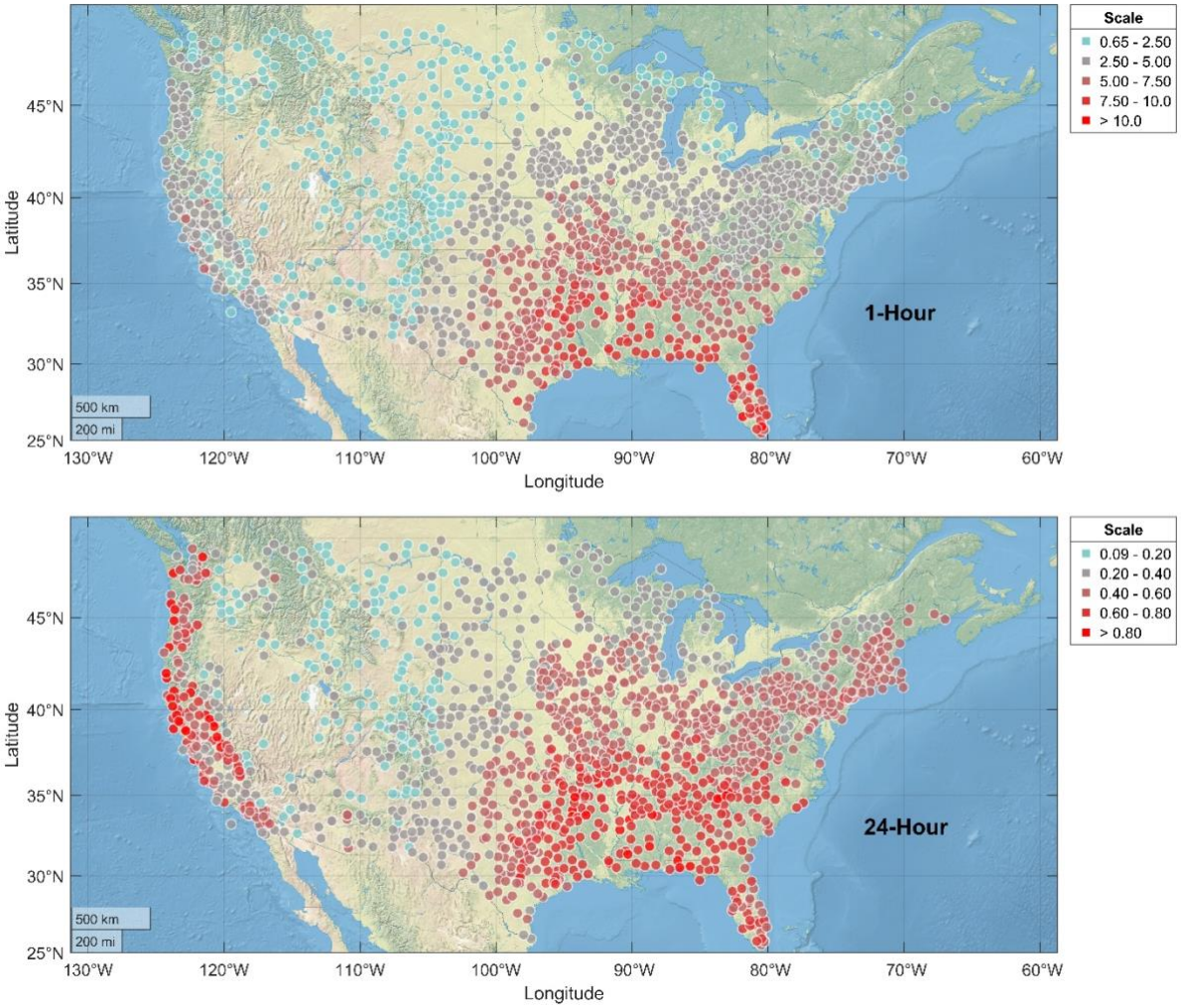

Figure 6 - Scale Parameters (in mm h^{-1}) for ordinary events of 1 and 24-hour time window obtained from a stretched exponential (Weibull) fitting of the ordinary events tail. Red color indicates larger values of scale, while cyan indicates smaller. The color scale is different for upper and lower panels because the different durations generate peak intensities of different order of magnitudes.

The scale parameters for stations over CONUS are displayed in Figure 6. We can observe that there is a gradient of increasing scale parameter for the 1-hour time window from northwest (0-2.5) to southeast (≥ 7.5). This pattern is not present in the 24-hour time window (bottom panel of Figure 6), where the scale values of the west coast are similar to the ones obtained for the southeast (≥ 0.80). This behavior highlights the precipitation patterns of the two regions. Intense short-duration events occur often in the Southeast during the summer and early fall, while the precipitation on the west coast is dominated by winter and spring events coming from the Pacific Ocean. It is worth noting that the order of magnitude of scale values is different for 1-hour and 24-hour time window events.

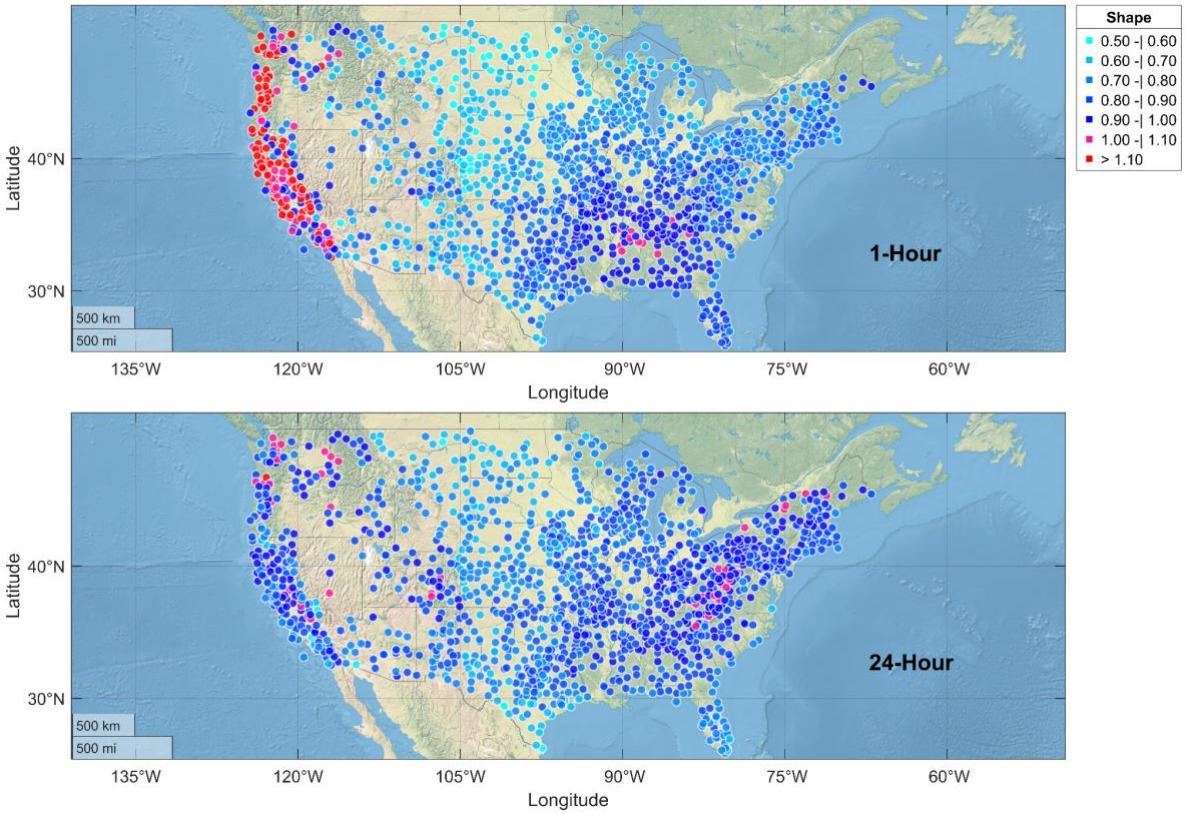

Figure 7 - Shape Parameters for ordinary events of 1 and 24-hour time window from a stretched exponential (Weibull) fitting of the ordinary events tail. Red and pink colors indicate shape values > 1 (light tail), while blue values indicate otherwise (heavy tail), with lighter colors indicating smaller values.

The shape parameters for stations over CONUS are displayed in Figure 7. Light tails are observed on the west coast of CONUS (shape values ≥ 1.0) for 1-hour time window. This is not observed for 24-hour window, for which the west coast has heavier tails that are comparable with the rest of CONUS (also see upper panels of Figure 8). The climate zones Csa and Csb, located on the west coast, show median shape values >1 for 1-hour and around 0.80 for 24-hour, which indicate tails heavier than exponential. The shape derived for 24-hour time window does not vary significantly across the regions (Figure 8, upper right), which suggests that, CONUS wide, the daily extremes are associated with similar combinations of precipitation processes. This is not the case for 1-h time windows. The regions Csa and Csb have lighter tails (larger shape parameters), as opposed to other regions. This implies that hourly extremes could be associated with diverse combinations of processes across CONUS. In fact, results displayed in Figures S3 and S4 shows that 25-60% of the events associated with the tail are different from 1 to 24-h, demonstrating that different proportions of precipitation processes are associated with each time window. The central portion of CONUS, covering the whole extent of the Great Plains, is characterized by heavier tails, with most stations indicating shape parameters between 0.5 and 0.7 for both durations (Figure 6). This behavior can be confirmed by analyzing the shape parameters for the climate zone BS in Figure 8, which presents a median value of 0.7 for 1-hour and 0.75 for 24-hour. The Great Plains are characterized by the formation of mesoscale convective systems during summer and fall seasons (Ashley et al.,

2003), which seem to have significant influence on the regional rainfall extremes. The shape parameter values are also consistent between time windows for the Southeast, represented by the climate zone Cf (Figure 8), with median values around 0.85. This consistency can indicate that the tails for both time windows are composed by a common group of storms (24-hour peaks may often derive from short-duration extremes). The northeastern region shows a decrease in tail heaviness for longer time windows, with most stations being in the 0.60-0.80 range for 1-hour and 0.80-0.90 for 24-hour windows (Figure 6). The region is represented by Climate Types Dfa and Dfb, which presents a median shape value of 0.75 (0.85) and 0.75 (0.9) for 1-hour (24-hour) respectively (Figure 8).

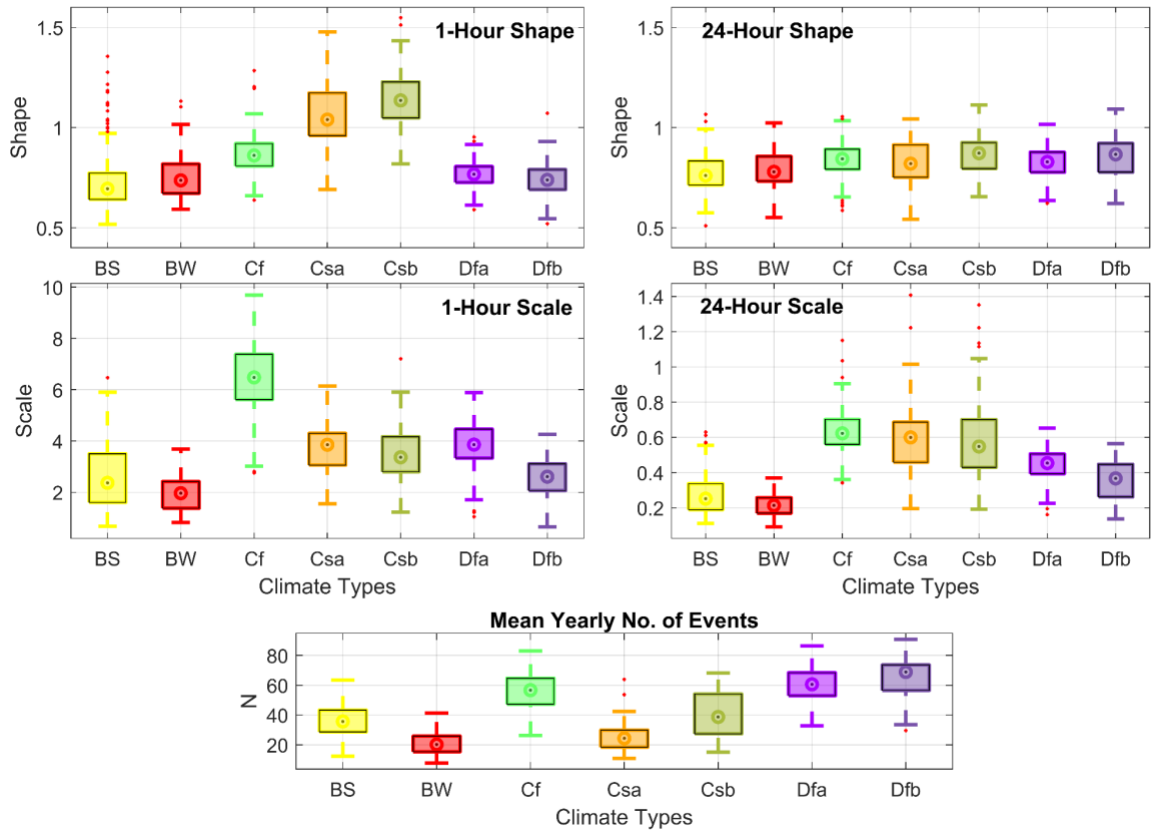

Figure 8 - Parameters of the Weibull distributions describing the tail of ordinary events of 1 and 24h time window considering different climate zones of CONUS. The y-axis is different for scale plots of 1 and 24-hour because the different durations generate peak intensities of different orders of magnitude. The climate types are: BS (yellow) - Arid Steppe climate; BW (red) - Arid Desert climate; Cf (green) - Temperate climate without dry season; Csa (orange) - Temperate climate with dry and hot summer; Csb (dark green) - Temperate climate with dry and warm summer; Dfa (light purple) - Cold climate without dry season and hot summer; Dfb (dark purple) - Cold climate without dry season and warm summer.

4.3. Storm properties in different climate zones

The analysis of storm characteristics can provide useful information on the relation between the statistics of extreme precipitation and the underlying physical processes. We extracted a set of properties from the 1-h and 24-h time window events which exceeded the 90th percentile of the ordinary events (mean duration, mean intensity, maximum intensity, decorrelation time) at

each station. This common threshold is chosen to provide comparability of the properties across stations. Although the value of threshold is common, the storms in 1h and 24h tail are not the same, as the heaviest storms can be different for different time windows (Figure S3 and S4). This implies that the reported differences between 1h and 24 statistics are attributed both to inter-storm variability and to intra-storm scaling, although the exact contributions of the two cannot be quantified. Their distribution across the different climate zones of CONUS is illustrated in Figure 9. The west coast, represented by the climate zones Csa and Csb, has extreme events of longer duration, indicating that large-scale atmospheric processes tend to dominate the tail. The decorrelation time of intense storms in these regions is also larger, highlighting a possible tendency for non-convective-like processes. Mean and Maximum intensity show similar relative patterns between climate zones, with the Cf zone showing larger values, illustrating the role of intense and short-duration extremes over the region. The BS and BW climate zones have short-duration events with relatively low intensities and short decorrelation time. The regions classified as Dfa and Dfb also have short-duration events with relatively high intensities and a very small variability in the decorrelation time, with a median of ~ 3 hours.

The ratio of convective-like storms (as defined in Section 3.4) is displayed in the bottom panel of Figure 9. For the 1-h time window, the ratio is around 0.8 for almost all climate regions, indicating that the tail properties are dominated by convective-like storms. The Csa and Csb climate zones provide an exception to this, with much lower ratios (around 0.4). This result corresponds with other storm properties associated with convective-like characteristics, that show intense, short-duration and short decorrelation time in the storms associated with the tail. The ratio of convective-like storms producing the maximum 24-h time intensity is much lower, confirming that different rainfall generation processes are present for longer time windows peak intensities. However, even for 24-h time window, over half of the stations still indicate tails dominated by convective-like storms, although this is almost entirely absent in the Csa and Csb regions.

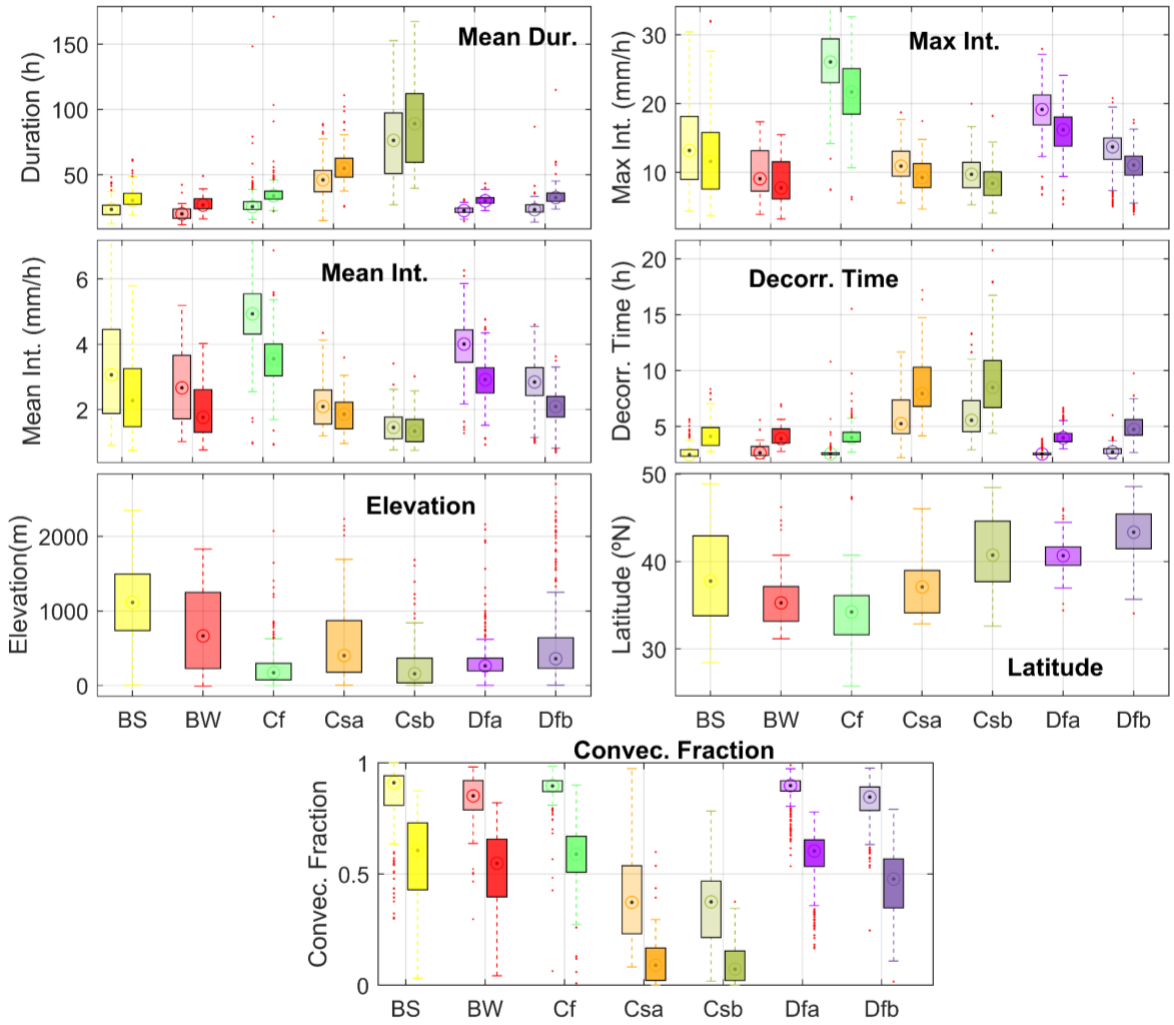

Figure 9 - Storm (ordinary events) characteristics above the 90th percentile considering the different climate zones of CONUS. The climate types are BS (yellow) - Arid Steppe climate; BW (red) - Arid Desert climate; Cf (green) - Temperate climate without dry season; Csa (orange) - Temperate climate with dry and hot summer; Csb (dark green) - Temperate climate with dry and warm summer; Dfa (light purple) - Cold climate without dry season and hot summer; Dfb (dark purple) - Cold climate without dry season and warm summer. Darker shades indicate values for 24-h time window, while lighter shades indicate 1-h. It is worth noting that the y-scale of the subplots corresponding to mean and maximum intensity are different.

Information on the hour of the day and seasonality of storm events is displayed on Figures S1 and S2 of the supplementary information. There, we can see that afternoon and early night (12pm to 12am) events are more common in most of the stations. The west coast has tail events associated with winter precipitation, whereas the rest of CONUS is spring/summer dominated.

4.4. Correlation between storm properties and shape parameter

The correlation between the storm properties and the shape parameter has revealed important features of the physical processes associated with the tails. Convective-like characteristics were demonstrated to have a link with tail heaviness, where increasing convective characteristics implied heavier tails, i.e., increased probability of extreme events.

394 The shape parameter shows a moderate positive correlation with the mean duration of the
395 storms associated with 1-hour extremes for the whole CONUS (0.53) and a weak correlation
396 for most of the climate zones separately (0.27-0.44) (Figure 10), with the Cf (0.07) and Dfa
397 (0.13) zones showing no correlation. A similar link is observed between storm duration and the
398 shape parameter for 24-hour time window, with a weak correlation for most regions (0.23-
399 0.34) and no correlation for Cf (0.01) and Csa (0.16). The maximum and mean intensities do
400 not show significant correlations with the shape parameter for 1-h time windows, and show
401 weak to moderate correlations for 24-h. The BW climate zone is the only one that presents a
402 notable and significant relationship between the shape parameter and 1-h time window peak
403 rainfall intensity, with a correlation of -0.46 and -0.51 for maximum and mean intensity
404 respectively. Decorrelation time shows a positive correlation with the shape parameter for both
405 windows considered for ordinary events, with coefficients indicating a weak correlation (0.29
406 for 1-hour and 0.41 for 24-hour). Although the correlation metrics range from weak to
407 moderate, they show a significant link of the storm properties with the shape parameter,
408 indicating that intense, short-duration events with short decorrelation times result in smaller
409 values for the shape parameter, i.e. heavier tailed distributions.

410 The overall negative correlation of the shape parameter with intensities and convective
411 fraction, and the positive trend with decorrelation time, suggests the possible role of convection
412 in increasing tail heaviness. Considering the entire CONUS, a correlation of -0.39 was obtained
413 for both durations. The values per climate zone vary from -0.43 to -0.13 for 1-h, and -0.61 to
414 0.26 for 24-h. This suggests a general agreement in the effect of an increase in convective-like
415 processes on decreasing the shape parameter.

416 Elevation and latitude have different effects on the shape parameter depending on the time
417 window duration and climate region. The correlation coefficients vary from -0.39 to 0.25 for
418 elevation and from -0.53 to 0.52 for latitude. For the 1-hour time window over CONUS, both
419 elevation and latitude have a weak negative correlation with the shape parameter, at -0.39 and
420 -0.33 respectively. This behavior is not observed for the 24-hour time window, which presents
421 coefficients of -0.16 and 0.07 respectively. The fact that stronger relationships are found for 1-
422 hour indicates that latitude and elevation have a greater influence on processes driving short-
423 duration extremes. The variability in the sign of correlation between climate zones, however,
424 indicates that there are stronger factors than elevation and latitude influencing the shape
425 parameter. Amponsah et al., (2022) found a positive relationship of elevation and latitude with
426 shape parameters obtained from daily precipitation in Ghana. The results differ from the ones
427 obtained for CONUS, but they are comparable with the results obtained here for the Temperate
428 Climate Zone (Cf) considering the time window of 24h, 0.2 for elevation and 0.52 for latitude.
429 Ghana is classified as tropical, which shares similarities (i.e., hot, and humid summer) with the
430 Cf region. The difference in spatial scales between CONUS and Ghana can also explain the
431 discrepancy in the results, indicating that the relationship is influenced by factors other than
432 elevation when considering continent-sized areas. In fact, when considering a smaller area
433 focused on the mountainous region of North Carolina (Figure S7), we obtained a correlation
434 coefficient of 0.35 for elevation-shape and 0.12 for latitude-shape. Results obtained by Marra

et al., (2021) corroborate with this statement, where a positive relationship was found for a focused area on the southeastern Mediterranean, between the Mediterranean and the dead sea.

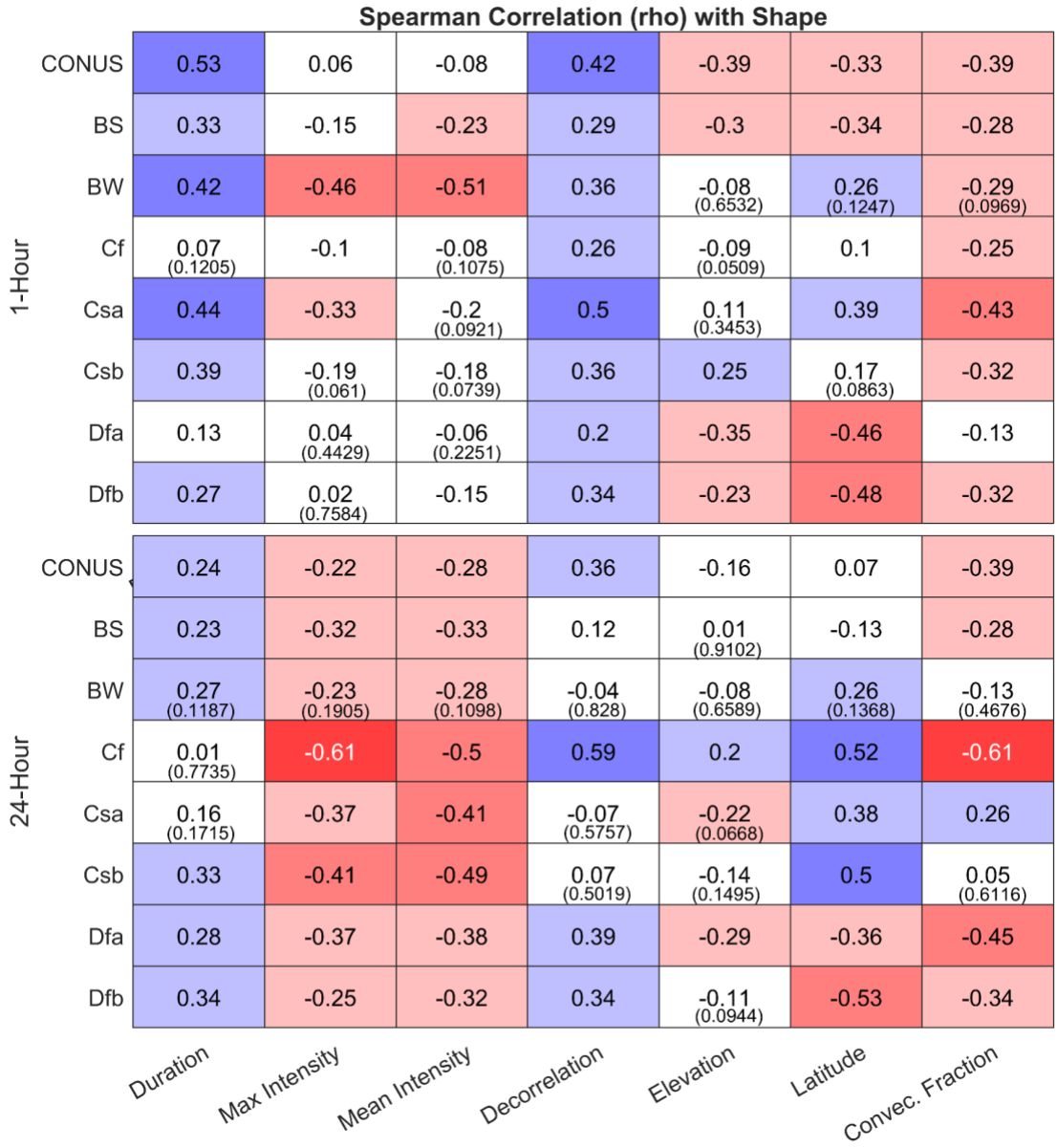

Figure 10 - Variability in the Spearman Correlation of 1 and 24-h time window (ordinary events) characteristics and the shape parameter for different climate zones over CONUS. Blue colors indicate positive correlation while red colors indicate negative. Most values are significant at the 95% confidence level (p-value < 0.05), the values that are outside this CI have the p-values displayed in parentheses.

4.4. Correlation between storm properties and scale parameter

An investigation of the relationship between storm properties and the scale parameter revealed stronger correlations than those for the shape parameter. We found a weak positive correlation for mean duration considering 24-h time window events for the whole CONUS (0.29) and a moderate correlation for the Csa (0.57) and Csb (0.46) climate zones. There is no link observed between the mean storm duration and the scale parameter for the 1-h time

window events, with the exception of a weak negative correlation (-0.25) for the BS climate zone. The maximum and mean intensities show a strong correlation with scale for 1-hour time window events over CONUS (0.88 for maximum and 0.74 for mean) and for most of the climate zones (0.72-0.87 and 0.49-0.7, respectively); however, values are lower (0.11-0.64) for the 24-hour time window. Decorrelation time shows no significant link when considering the entire CONUS, but there are strong relationships with the scale parameter for specific climate zones, such as for Csa (0.71) and Csb (0.74).

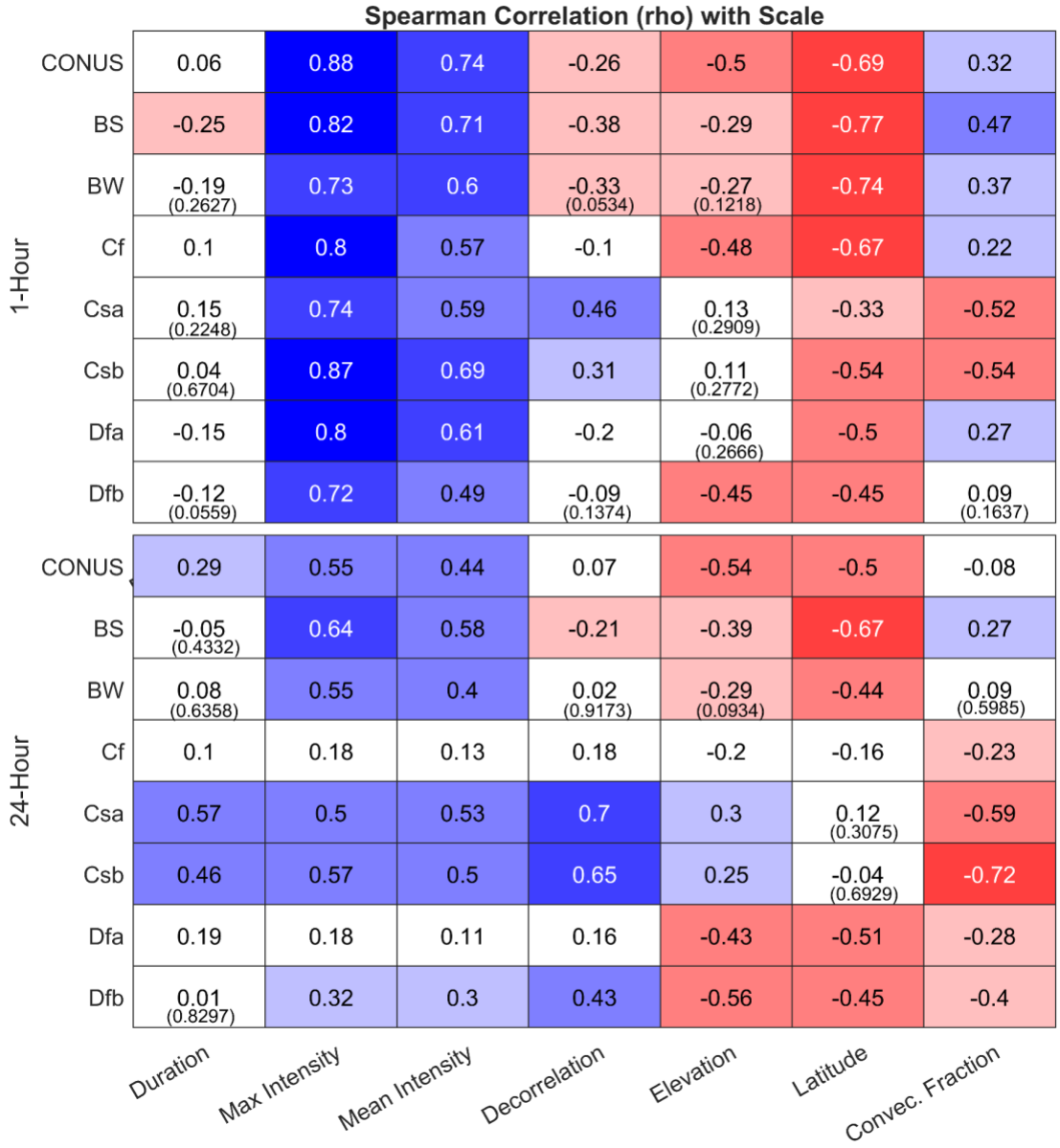

Figure 11 - Variability in the correlation metrics of 1 and 24-h time window (ordinary events) characteristics and the scale parameter for different climate zones over CONUS. Blue colors indicate positive correlation while red colors indicate negative. Most values are significant at the 95% confidence level (p-value < 0.05), the values that are outside this CI have the p-values displayed in parentheses.

Elevation and latitude are a significant factor of influence on the scale parameter, both for 1- and 24-hour time windows. The correlation coefficients obtained for CONUS were -0.5 (-0.54)

and -0.69 (-0.5) for 1-h (24-h) for elevation and latitude respectively. Amponsah et al., (2022) found positive relationship of the scale parameter with latitude and no significant relationship between elevation and scale for a tropical climate zone in Sub-Saharan Africa, differing from our results. However, Marra et. al., (2021) found a negative relationship between scale and elevation for a region in the southeastern Mediterranean, in agreement with our findings. These results emphasize the role of other major factors, such as climate characteristics, in the relationship of geographic properties and tail statistics.

5. Conclusions

In this study we used a statistical framework based on the concept of ordinary events, here defined as the maximum intensities of storm events over two time windows (1 and 24-h), to analyze the influence of storm properties on the statistics of extreme precipitation. A two-parameter Weibull distribution was used to represent precipitation frequencies at several stations from the GSDR dataset (Lewis et al., 2019) over CONUS, encompassing seven climate zones. Our results reveal significant (at the 95% confidence level) relationships between storm properties and the statistics of extreme precipitation.

Our analysis indicated that the stretched exponential (two-parameter Weibull) is a suitable distribution to represent the ordinary events over CONUS. Considering the robustness of the applied test in comparison with alternative tail models (e.g., power-type and Generalized Pareto), our results also demonstrate the viability of a stretched-exponential tail framework for hourly precipitation. The proportion of ordinary events belonging to the tail, represented by the left-censoring threshold, is a climate property, with higher values of the threshold (less events in the tails) in the Northwest and Northeast of CONUS. Overall, the threshold is lower when a longer time window (24h) is considered.

The parameters obtained from the fitted distribution offered useful insights into the spatial distribution of precipitation extremes. The shape parameter revealed lighter tails on the west coast for the 1-h time window events. Heavier tails were found in the central region of CONUS, indicating larger probabilities of extreme precipitation in that region. The scale parameter showed large variation from 1-h to 24-h time window events for the west coast. At 24-h duration, the scale parameters of the west coast have similar values as the Eastern region, while this behavior is not observed at 1-h.

The storm properties tested showed significant correlations with properties of the ordinary events distribution (the shape and scale parameters). The ratio of convective-like storms, and the average maximum and mean storm intensities have a positive correlation with the tail heaviness, which indicates that increasing convective fraction likely translates into heavier tails. The positive link with storm duration and decorrelation time corroborated these results. Elevation and latitude presented weak to moderate correlation with the distribution parameters for the entire CONUS, even more for climate zones on the eastern coast. Correlation coefficients were stronger between storm properties and the scale parameter than for the shape parameter, presenting a significant strong correlation with latitude, and maximum and mean intensities. These relationships provide useful information on relation of storm properties and

storm parameters over CONUS, contributing to an increase in overall knowledge of the statistical analysis of extreme events.

Acknowledgements

Araujo and Nikolopoulos were supported by the National Science Foundation, United States, under Grant No. (2243809). Marra was supported by the CARIPARO Foundation through the Excellence Grant 2021 to the "Resilience" Project. We would like to acknowledge (Marra, 2022; Marra et al., 2023) for developing and sharing the scripts for the hypothesis test for the Weibull tail.

References

Ali, H., Fowler, H. J., Lenderink, G., Lewis, E., & Pritchard, D. (2021). Consistent large-scale response of hourly extreme precipitation to temperature variation over land. *Geophysical Research Letters*, *48*(4). https://doi.org/10.1029/2020gl090317

Ali, H., Fowler, H. J., Pritchard, D., Lenderink, G., Blenkinsop, S., & Lewis, E. (2022). Towards quantifying the uncertainty in estimating observed scaling rates. *Geophysical Research Letters*, *49*(12), e2022GL099138.

Amponsah, W., Dallan, E., Nikolopoulos, E. I., & Marra, F. (2022). Climatic and altitudinal controls on rainfall extremes and their temporal changes in data-sparse tropical regions. *Journal of Hydrology*, *612*, 128090.

Ashley, W. S., Mote, T. L., Grady Dixon, P., Trotter, S. L., Powell, E. J., Durkee, J. D., & Grundstein, A. J. (2003). Distribution of Mesoscale Convective Complex Rainfall in the United States. *Monthly Weather Review*, *131*(12), 3003–3017.

Barbero, R., Westra, S., Lenderink, G., & Fowler, H. J. (2018). Temperature-extreme precipitation scaling: a two-way causality? *International Journal of Climatology: A Journal of the Royal Meteorological Society*, *38*(S1), e1274–e1279.

Blenkinsop, S., Fowler, H. J., Barbero, R., Chan, S. C., Guerreiro, S. B., Kendon, E., Lenderink, G., Lewis, E., Li, X.-F., Westra, S., Alexander, L., Allan, R. P., Berg, P., Dunn, R. J. H., Ekström, M., Evans, J. P., Holland, G., Jones, R., Kjellström, E., …

Tye, M. R. (2018). The INTENSE project: using observations and models to understand the past, present and future of sub-daily rainfall extremes. *Advances in Science and Research*, *15*, 117–126.

Cooley, A. K., & Chang, H. (2020). Detecting change in precipitation indices using observed (1977–2016) and modeled future climate data in Portland, Oregon, USA. *Journal of Water and Climate Change*, *12*(4), 1135–1153.

Dallan, E., Borga, M., Zaramella, M., & Marra, F. (2022). Enhanced summer convection explains observed trends in extreme subdaily precipitation in the Eastern Italian alps. *Geophysical Research Letters*, *49*(5). https://doi.org/10.1029/2021gl096727

Fisher, R. A., & Tippett, L. H. C. (1928). Limiting forms of the frequency distribution of the largest or smallest member of a sample. *Mathematical Proceedings of the Cambridge Philosophical Society*, *24*(2), 180–190.

Formetta, G., Marra, F., Dallan, E., Zaramella, M., & Borga, M. (2022). Differential orographic impact on sub-hourly, hourly, and daily extreme precipitation. *Advances in Water Resources*, *159*, 104085.

Gershunov, A. (1998). ENSO Influence on Intraseasonal Extreme Rainfall and Temperature Frequencies in the Contiguous United States: Implications for Long-Range Predictability. *Journal of Climate*, *11*(12), 3192–3203.

Ghada, W., Casellas, E., Herbinger, J., Garcia-Benadí, A., Bothmann, L., Estrella, N., Bech, J., & Menzel, A. (2022). Stratiform and Convective Rain Classification Using Machine Learning Models and Micro Rain Radar. *Remote Sensing*, *14*(18), 4563.

Gnedenko, B. (1943). Sur La Distribution Limite Du Terme Maximum D'Une Serie Aleatoire. *Annals of Mathematics*, *44*(3), 423–453.

Higgins, R. W., Yao, Y., & Wang, X. L. (1997). Influence of the North American Monsoon System on the U.S. Summer Precipitation Regime. *Journal of Climate*, *10*(10), 2600–

554 2622.
555 Hu, L., Nikolopoulos, E. I., Marra, F., Morin, E., Marani, M., & Anagnostou, E. N. (2020).
556 Evaluation of MEVD-based precipitation frequency analyses from quasi-global
557 precipitation datasets against dense rain gauge networks. *Journal of Hydrology*, *590*,
558 125564.
559 Huang, J., Fatichi, S., Mascaro, G., Manoli, G., & Peleg, N. (2022). Intensification of sub-
560 daily rainfall extremes in a low-rise urban area. *Urban Climate*, *42*, 101124.
561 Katz, R. W., Parlange, M. B., & Naveau, P. (2002). Statistics of extremes in hydrology.
562 *Advances in Water Resources*, *25*(8), 1287–1304.
563 Kim, S., Sharma, A., Wasko, C., & Nathan, R. (2022). Linking total precipitable water to
564 precipitation extremes globally. *Earth's Future*, *10*(2).
565 https://doi.org/10.1029/2021ef002473
566 Knight, D. B., & Davis, R. E. (2007). Climatology of Tropical Cyclone Rainfall in the
567 Southeastern United States. *Physical Geography*, *28*(2), 126–147.
568 Kunkel, K. E., Karl, T. R., Squires, M. F., Yin, X., Stegall, S. T., & Easterling, D. R. (2020).
569 Precipitation Extremes: Trends and Relationships with Average Precipitation and
570 Precipitable Water in the Contiguous United States. *Journal of Applied Meteorology*
571 *and Climatology*, *59*(1), 125–142.
572 Lewis, E., Fowler, H., Alexander, L., Dunn, R., McClean, F., Barbero, R., Guerreiro, S., Li,
573 X.-F., & Blenkinsop, S. (2019). GSDR: A Global Sub-Daily Rainfall Dataset. *Journal*
574 *of Climate*, *32*(15), 4715–4729.
575 Lewis, E., Pritchard, D., Villalobos-Herrera, R., Blenkinsop, S., McClean, F., Guerreiro, S.,
576 Schneider, U., Becker, A., Finger, P., Meyer-Christoffer, A., Rustemeier, E., &
577 Fowler, H. J. (2021). Quality control of a global hourly rainfall dataset.
578 *Environmental Modelling & Software*, *144*, 105169.

Li, M., Sun, Q., Lovino, M. A., Ali, S., Islam, M., Li, T., Li, C., & Jiang, Z. (2022). Non-uniform changes in different daily precipitation events in the contiguous United States. *Weather and Climate Extremes*, *35*, 100417.

Lopez-Cantu, T., Prein, A. F., & Samaras, C. (2020). Uncertainties in future U.s. extreme precipitation from downscaled climate projections. *Geophysical Research Letters*, *47*(9), e2019GL086797.

Marani, M., & Ignaccolo, M. (2015). A metastatistical approach to rainfall extremes. *Advances in Water Resources*, *79*, 121–126.

Marra, F., Amponsah, W., & Papalexiou, S. M. (2023). *Non-asymptotic Weibull tails explain the statistics of extreme daily precipitation*.

Marra, Francesco. (2022). *A test for the hypothesis: block maxima are samples from a parent distribution with Weibull tail*. https://doi.org/10.5281/zenodo.7234708

Marra, Francesco, Armon, M., Adam, O., Zoccatelli, D., Gazal, O., Garfinkel, C. I., Rostkier-Edelstein, D., Dayan, U., Enzel, Y., & Morin, E. (2021). Toward narrowing uncertainty in future projections of local extreme precipitation. *Geophysical Research Letters*, *48*(5). https://doi.org/10.1029/2020gl091823

Marra, Francesco, Armon, M., Borga, M., & Morin, E. (2021). Orographic effect on extreme precipitation statistics peaks at hourly time scales. *Geophysical Research Letters*, *48*(5). https://doi.org/10.1029/2020gl091498

Marra, Francesco, Borga, M., & Morin, E. (2020a, June 26). *A Unified Framework for Extreme Sub-daily Precipitation Frequency Analyses based on Ordinary Events*. https://doi.org/10.1002/essoar.10503502.1

Marra, Francesco, Borga, M., & Morin, E. (2020b). A unified framework for extreme subdaily precipitation frequency analyses based on ordinary events. *Geophysical Research Letters*, *47*(18). https://doi.org/10.1029/2020gl090209

604 Marra, Francesco, Levizzani, V., & Cattani, E. (2022). Changes in extreme daily precipitation
605 over Africa: Insights from a non-asymptotic statistical approach. *Journal of*
606 *Hydrology X*, *16*, 100130.
607 Marra, Francesco, Nikolopoulos, E. I., Anagnostou, E. N., & Morin, E. (2018).
608 Metastatistical Extreme Value analysis of hourly rainfall from short records:
609 Estimation of high quantiles and impact of measurement errors. *Advances in Water*
610 *Resources*, *117*, 27–39.
611 Marra, Francesco, Zoccatelli, D., Armon, M., & Morin, E. (2019). A simplified MEV
612 formulation to model extremes emerging from multiple nonstationary underlying
613 processes. *Advances in Water Resources*, *127*, 280–290.
614 Martinez-Villalobos, C., & Neelin, J. D. (2018). Shifts in precipitation accumulation
615 extremes during the warm season over the United States. *Geophysical Research*
616 *Letters*, *10*(2), 8586–8595.
617 Mazzoglio, P., Butera, I., Alvioli, M., & Claps, P. (2022). The role of morphology in the
618 spatial distribution of short-duration rainfall extremes in Italy. *Hydrology and Earth*
619 *System Sciences*, *26*(6), 1659–1672.
620 Miniussi, A., & Marani, M. (2020). Estimation of daily rainfall extremes through the
621 metastatistical extreme value distribution: Uncertainty minimization and implications
622 for trend detection. *Water Resources Research*, *56*(7).
623 https://doi.org/10.1029/2019wr026535
624 Miniussi, A., & Marra, F. (2021). Estimation of extreme daily precipitation return levels at-
625 site and in ungauged locations using the simplified MEV approach. *Journal of*
626 *Hydrology*, *603*, 126946.
627 Miniussi, A., Villarini, G., & Marani, M. (2020). Analyses through the metastatistical
628 extreme value distribution identify contributions of tropical cyclones to rainfall

629 extremes in the Eastern United States. *Geophysical Research Letters*, *47*(7),
630 e2020GL087238.
631 Moore, B. J., White, A. B., & Gottas, D. J. (2021). Characteristics of Long-Duration Heavy
632 Precipitation Events along the West Coast of the United States. *Monthly Weather*
633 *Review*, *149*(7), 2255–2277.
634 Papalexiou, S. M., AghaKouchak, A., & Foufoula-Georgiou, E. (2018). A diagnostic
635 framework for understanding climatology of tails of hourly precipitation extremes in
636 the United States. *Water Resources*, *54*(9), 6725–6738.
637 Peel, M. C., Finlayson, B. L., & McMahon, T. A. (2007). Updated world map of the Köppen-
638 Geiger climate classification. *Hydrology and Earth System Sciences*, *11*(5), 1633–
639 1644.
640 Prein, A. F., Rasmussen, R. M., Ikeda, K., Liu, C., Clark, M. P., & Holland, G. J. (2016). The
641 future intensification of hourly precipitation extremes. *Nature Climate Change*, *7*(1),
642 48–52.
643 Schellander, H., Lieb, A., & Hell, T. (2019). Error structure of metastatistical and generalized
644 extreme value distributions for modeling extreme rainfall in Austria. *Earth and Space*
645 *Science (Hoboken, N.J.)*, *6*(9), 1616–1632.
646 Serinaldi, F., & Kilsby, C. G. (2014). Rainfall extremes: Toward reconciliation after the
647 battle of distributions. *Water Resources Research*, *50*(1), 336–352.
648 Sui, C.-H., Tsay, C.-T., & Li, X. (2007). Convective–stratiform rainfall separation by cloud
649 content. *Journal of Geophysical Research*, *112*(D14).
650 https://doi.org/10.1029/2006jd008082
651 Thurai, M., Wolff, D., Marks, D., Pabla, C., & Bringi, V. (2021). Separation of Stratiform
652 and Convective Rain Types Using Data from an S-Band Polarimetric Radar: A Case
653 Study Comparing Two Different Methods. *Environmental Sciences Proceedings*,

654 *8*(1), 1.
655 Treppiedi, D., Cipolla, G., & Noto, L. V. (2022). Convective precipitation over a
656 Mediterranean area: From identification to trend analysis starting from high-
657 resolution rain gauges data. *International Journal of Climatology*.
658 https://doi.org/10.1002/joc.7758
659 Vidrio-Sahagún, C. T., & He, J. (2022). Hydrological frequency analysis under
660 nonstationarity using the Metastatistical approach and its simplified version. *Advances*
661 *in Water Resources*, *166*, 104244.
662 Vidrio-Sahagún, C. T., He, J., & Pietroniro, A. (2023). Nonstationary hydrological frequency
663 analysis using the Metastatistical extreme value distribution. *Advances in Water*
664 *Resources*, *176*(104460), 104460.
665 Wang, Y., Tang, L., Chang, P.-L., & Tang, Y.-S. (2021). Separation of convective and
666 stratiform precipitation using polarimetric radar data with a support vector machine
667 method. *Atmospheric Measurement Techniques*, *14*(1), 185–197.
668 Zhu Jianting. (2013). Impact of Climate Change on Extreme Rainfall across the United
669 States. *Journal of Hydrologic Engineering*, *18*(10), 1301–1309.
670 Zhu, W., Wang, S., Luo, P., Zha, X., Cao, Z., Lyu, J., Zhou, M., He, B., & Nover, D. (2022).
671 A Quantitative Analysis of the Influence of Temperature Change on the Extreme
672 Precipitation. *Atmosphere*, *13*(4), 612.
673 Zorzetto, E., Botter, G., & Marani, M. (2016). On the emergence of rainfall extremes from
674 ordinary events. *Geophysical Research Letters*, *43*(15), 8076–8082.
675